Near-Exact Analytical Solution of the Sir-Model for the Precise Temporal Dynamics of Epidemics

Martin Kröger * and Reinhard Schlickeiser

Posted Date: 7 November 2024

doi: 10.20944/preprints202411.0521.v1

Keywords: coronavirus; statistical analysis; Covid-19; pandemic spreading; nonlinear differential equation

 doi:10.20944/preprints202411.0521.v1

Article

Near-Exact Analytical Solution of the SIR-Model for the Precise Temporal Dynamics of Epidemics

Reinhard Schlickeiser [1,2,*] **and Martin Kröger** [3,4,*]

[1] Institut für Theoretische Physik, Lehrstuhl IV: Weltraum- und Astrophysik, Ruhr-Universität Bochum, D-44780 Bochum, Germany
[2] Institut für Theoretische Physik und Astrophysik, Christian-Albrechts-Universität zu Kiel, Leibnizstr. 15, D-24118 Kiel, Germany
[3] Magnetism and Interface Physics, Department of Materials, ETH Zurich, Zurich CH-8093, Switzerland
[4] Computational Polymer Physics, Department of Materials, ETH Zurich, Zurich CH-8093, Switzerland
* Correspondence: rsch@tp4.rub.de (R.S.); mk@mat.ethz.ch (M.K.)

Abstract: A near-exact analytical solution of the statistical Susceptible-Infectious-Recovered (SIR) epidemics model for a constant ratio k_0 of infection to recovery rates is derived. The derived solution is not of inverse form as the known solutions in the literature but expresses rather directly the three compartmental fractions $S(\tau)$, $I(\tau)$ and $R(\tau)$ and thus the rate of new infections $j(\tau) = S(\tau)I(\tau)$ in terms of the single function $U(\tau)$ and the reduced time τ (the time-integrated infection rate), involving the principal and non-principal branches of Lambert's function. Exact analytical formulas for the peak time and the maximum fraction of $I(\tau)$ are obtained proving that the rate of new infections peaks before the fraction of infected persons. Our analysis is not entirely analytically exact because the reduced time dependence of the function $U(\tau)$ obeying a nonlinear integro-differential equation is only obtained approximately by expanding a double-exponential function to first-order at small reduced times, and employing an accurate simple approximation of the principal Lambert function at large times, respectively.

Keywords: coronavirus; statistical analysis; Covid-19; pandemic spreading

1. Introduction

The Susceptible-Infectious-Recovered (SIR) model is the simplest of the compartmental models used for the mathematical modeling of infectious diseases in order to reproduce or predict the temporal evolution of infectious diseases in human populations. Originally developed nearly hundred years ago [1,2] it lately has become very popular and widespread [3–43] due to its successful applications to the outbreaks of the corona virus in many countries [44]. The considered population of $N \gg 1$ initially susceptible persons is assigned to the three compartments $S(t)$ (susceptible), $I(t)$ (infectious), or $R(t)$ (recovered/removed). Persons from the population may progress between these compartments described by the time-dependent infection ($a(t)$ and recovery ($\mu(t)$) rates.

The three respective population fractions obey the sum constraint condition

$$I(t) + S(t) + R(t) = 1 \tag{1}$$

at any time, and their temporal evolution is given by the SIR-equations

$$\frac{dS(t)}{dt} = -a(t)S(t)I(t), \tag{2a}$$

$$\frac{dI(t)}{dt} = a(t)S(t)I(t) - \mu(t)I(t), \tag{2b}$$

$$\frac{dR(t)}{dt} = \mu(t)I(t). \tag{2c}$$

Besides numerical solutions it is of high interest to derive analytical solutions of the underlying dynamical SIR-equations. In the most general case of a time-dependent ratio $k(t) = \mu(t)/a(t)$ between the recovery and the infection rate analytical approximate solutions were derived [45,46] which are

 doi:10.20944/preprints202411.0521.v1

very accurate if the cumulative fraction of infections $J(t) = 1 - S(t)$ is small compared to unity at all times.

Recently, new analytical solutions became available [47,48] for an arbitrary time dependence of the infection and recovery rates, provided that the ratio between the two rates is independent of time, for two different types of initial conditions. We refer to these in the following as KSSIR solutions. The utility of the KSSIR solutions were proven by their successful application to past waves of the corona virus [47]. However, in both cases the KSSIR solutions could only be given in inverse form $t(S)$ involving an integral, that had to be approximated by second-order polynomials (see [47] for details). Here we consider an alternative approach to the KSSIR solution that avoids the inverse form adopting the semi-time initial conditions [49–59]

$$S(0) = 1 - \eta, \qquad I(0) = \eta, \qquad R(0) = 0, \tag{3}$$

with $0 < \eta \simeq \mathcal{O}(1/N) \ll 1$ denoting the initial seed infection fraction of the population.

Two quantities are of particular interest in studies of infections [60–101]:

(1) the differential rate of newly infected persons from the desease

$$\dot{J}(t) = a(t)I(t)S(t), \tag{4}$$

which, with a delay time t_d of about a week, determines the death rate $d(t) = fNj(t - t_d)$, where the mortality rate f is of the order 10^{-2}–10^{-3} varying for different mutants of the Covid virus and different countries [102]. $\dot{J}(t)$ also determines the hospitalization rate of seriously infected persons.

(2) the fraction of infected persons $I(t)$ determines the peak time of required clinical resources in the host country of the considered population [103].

Both quantities $\dot{J}(t)$ and $I(t)$ first increase in time, undergo a maximum and drop at late times. While exact analytical formulas for the peak time τ_j and the peak rate of new infections $\dot{J}_{\max}$ are available in the KSSIR-model, several different approximations for the peak time τ_j and the peak fraction of infected persons $I_{\max}$ have been derived [103]. It is one purpose of the present study to derive exact expressions for τ_I and $I_{\max}$.

2. Reduction of the General SIR-Equations

By introducing the reduced time

$$\tau = \int_{t_0}^{t} d\xi\, a(\xi) \tag{5}$$

for arbitrary but given real time dependent infection rates $a(t)$ and the ratio

$$k(\tau(t)) = \frac{\mu(t)}{a(t)} \tag{6}$$

the SIR-equations (1)-(3) can be written as

$$\frac{dS(\tau)}{d\tau} = -S(\tau)I(\tau), \tag{7a}$$

$$\frac{dI(\tau)}{d\tau} = S(\tau)I(\tau) - k(\tau)I(t), \tag{7b}$$

$$\frac{dR(\tau)}{d\tau} = k(\tau)I(\tau), \tag{7c}$$

$$1 = S(\tau) + I(\tau) + R(\tau), \tag{7d}$$

 doi:10.20944/preprints202411.0521.v1

subject to initial conditions

$$S(\tau=0)=1-\eta, \quad I(\tau=0)=\eta, \quad R(\tau=0)=0. \tag{8}$$

From the invariant $\dot{J}(t)dt = j(\tau)d\tau$ we obtain with Equation (5) in the form $d\tau/dt = a(t)$ for the differential rate of newly infected persons from the desease

$$j(\tau)=\frac{dJ(\tau)}{d\tau}=\frac{\dot{J}(t)}{a(t)}=S(\tau)I(\tau)=-\frac{dS(\tau)}{d\tau} \tag{9}$$

with the initial value $j(0)=\eta(1-\eta)$. The invariant ($J(t)=J(\tau)$) cumulative distribution corresponding to $j(\tau)$ is given by

$$J(\tau)=\int_{-\infty}^{\tau}d\tau' j(\tau')=J(0)-\int_0^{\tau}d\tau'\frac{dS(\tau')}{d\tau'}=J(0)+S(0)-S(\tau)=1-S(\tau), \tag{10}$$

where the initial condition $J(0)=I(0)=\eta$ had been used, in accord with Equation (8).

2.1. Reduction

Equation (7a) readily yields

$$I(\tau) \;=\; -\frac{d\ln S(\tau)}{d\tau}=-\frac{dS(\tau)/d\tau}{S(\tau)}, \tag{11}$$

whereas Equation (7b) provides

$$\frac{d\ln I(\tau)}{d\tau} \;=\; S(\tau)-k(\tau), \tag{12}$$

which with the initial condition on $I(0)=\eta$ integrates to

$$I(\tau) \;=\; \eta e^{U(\tau)}, \tag{13}$$

$$U(\tau) \;=\; \int_0^{\tau}dx\,[S(x)-k(x)]. \tag{14}$$

Combining Equations (11) and (13) with

$$S(\tau) \;=\; \frac{dU(\tau)}{d\tau}+k(\tau) \tag{15}$$

then leads to the single nonlinear differential equation

$$\frac{d}{d\tau}\ln\left[\frac{dU(\tau)}{d\tau}+k(\tau)\right] \;=\; -\eta e^{U(\tau)} \tag{16}$$

for $U(\tau)$. Equation (16) integrates to

$$\frac{dU(\tau)}{d\tau}+k(\tau)=(1-\eta)\exp\left[-\eta\int_0^{\tau}dx\,e^{U(x)}\right], \tag{17}$$

where we made use of the initial condition $S(0)=1-\eta$.

2.2. Stationary Ratio

Throughout this study a stationary ratio (6) is assumed, i.e.,

$$k(\tau)=k_0=\text{const.} \tag{18}$$

 doi:10.20944/preprints202411.0521.v1

k_0 often is referred to as inverse reproduction number. The derived exact analytical solutions then hold for stationary infection and recovery rates as well as for any time-dependent infection rate $a(t)$ provided the recovery rate $\mu(t) \propto a(t)$ has the same time variation while its absolute value can be different.

For a stationary ratio Equations (14) and (16)–(17) simplify to

$$\begin{aligned} U(\tau) &= \int_0^\tau dx\, S(x) - k_0\tau, && \text{(19a)} \\ \frac{d}{d\tau}\ln\left[\frac{dU(\tau)}{d\tau} + k_0\right] &= -\eta e^{U(\tau)}, && \text{(19b)} \\ \frac{dU(\tau)}{d\tau} + k_0 &= (1-\eta)e^{-\eta\int_0^\tau dx\, e^{U(x)}}, && \text{(19c)} \\ \frac{d^2U(\tau)}{d\tau^2} &= -\eta(1-\eta)U(\tau)e^{-\eta\int_0^\tau dx\, e^{U(x)}}. && \text{(19d)} \end{aligned}$$

In earlier work [48] Equations (7) were solved exactly in inverse form as

$$\tau = \int_\eta^J \frac{dx}{(1-x)\left(x + k_0 \ln\frac{1-x}{1-\eta}\right)}, \tag{20}$$

allowing important conclusions on the final values of the fractions S, I, R (see Appendix A for details). Here we will follow a different approach avoiding the necessary inversion of solution (20) to derive $J(\tau)$. However, the noted exact results from Appendix A will be used below to check the validity of the alternative solution.

3. Exact Solution

3.1. Ansatz

The ansatz

$$\frac{dU(\tau)}{d\tau} + k_0 = -k_0 W\left(-ae^{be^{U(\tau)}}\right) \tag{21}$$

in terms of the Lambert [104] function $W(Z)$ (see Appendix G of ref. [105]) and yet unspecified constants a and b provides for Equation (19c)

$$-k_0 W(-ae^{be^{U(\tau)}}) = (1-\eta)e^{-\eta\int_0^\tau dx\, e^{U(x)}}. \tag{22}$$

Note that the ansatz (21) is equivalent to

$$-k_0\tau = \int^U \frac{dx}{1 + W(-ae^{be^x})}. \tag{23}$$

Next, we will determine the constants a and b and thus prove that the ansatz (21) fulfills the differential equation (19c). Applying the defining equation for the Lambert function

$$W(Z) = Ze^{-W(Z)} \tag{24}$$

yields for Equation (22)

$$\eta\int_0^\tau dx\, e^{U(x)} = W\left(-ae^{bU(\tau)}\right) - be^{U(\tau)} - \ln\left(\frac{k_0 a}{1-\eta}\right). \tag{25}$$

 doi:10.20944/preprints202411.0521.v1

Hence for its derivative with respect to τ, with

$$Z(\tau) \quad = \quad -ae^{be^{U(\tau)}}, \tag{26}$$

one obtains

$$\begin{aligned} \eta e^{U(\tau)} &= \frac{dU}{d\tau}\left[\frac{d}{dU}W(-ae^{be^U}) - be^U\right] = \frac{dU}{d\tau}\left[\frac{dZ}{dU}\frac{d}{dZ}W(Z) - be^U\right] \\ &= \frac{dU}{d\tau}\left[be^U Z\frac{d}{dZ}W(Z) - be^U\right] = \frac{dU}{d\tau}be^U\left[Z\frac{d}{dZ}W(Z) - 1\right] \\ &= \frac{dU}{d\tau}be^U\left[\frac{W(Z)}{1+W(Z)} - 1\right] = -\frac{dU}{d\tau}\frac{be^{U(\tau)}}{1+W(Z)}, \end{aligned} \tag{27}$$

where we used the differential equation

$$Z\frac{dW(Z)}{dZ} = \frac{W(Z)}{1+W(Z)} \tag{28}$$

for Lambert functions. The Equation (28) can be written as

$$-\frac{d\tau}{dU} = \frac{b/\eta}{1+W(Z)}, \tag{29}$$

which is solved by

$$-\tau = \frac{b}{\eta}\int^U \frac{dx}{1+W(-ae^{be^x})}. \tag{30}$$

In order for the solution (30) to be consistent with Equation (23) one has to demand that $b = \eta/k_0$. Consequently, the exact solution is given by

$$-k_0\tau = \int^U \frac{dx}{1+W\left(-ae^{\frac{\eta e^x}{k_0}}\right)}, \tag{31}$$

where we still have to determine the constant a and the lower integration limit from the initial condition and we have to identify the appropriate branch of the Lambert function.

If we re-use $U(0) = 0$ and $U'(0) = 1-\eta-k_0$, then we can determine a from Equation (27) evaluated at $\tau = 0$,

$$1 = -\frac{1-\eta-k_0}{k_0[1+W(-ae^{\eta/k_0})]}, \tag{32}$$

or equivalently

$$W(-ae^{\eta/k_0}) = -\frac{1-\eta}{k_0}. \tag{33}$$

With Equation (24) written as

$$Z = We^W, \tag{34}$$

Equation (33) can be solved for a and provides

$$a = \frac{(1-\eta)e^{-1/k_0}}{k_0} = -\alpha, \tag{35}$$

with α from Equation (A9) in Appendix A.

 doi:10.20944/preprints202411.0521.v1

To conclude, Equation (21) is formally solved by

$$\tau = -\frac{1}{k_0}\int^{U} \frac{dx}{1+W\left(-\frac{1-\eta}{k_0}e^{-(1-\eta e^x)/k_0}\right)} = -\frac{1}{k_0}\int^{U} \frac{dx}{1+W\left(\alpha e^{\frac{\eta e^x}{k_0}}\right)}, \tag{36}$$

but we have to make this more precise, as the Lambert function W has two branches, W_0 and W_{-1}.

For positive k_0 and $\eta \in [0,1)$ the argument of the Lambert function is negative because $\alpha < 0$. Recall that $W(Z) = -1$ for $Z = -1/e$, where the two Lambert branches meet. Let τ_U and $U_{\max}$ denote the peak time and peak amplitude of $U(\tau)$. The peak amplitude $U_{\max} = U(\tau_U)$ is determined by the solution of $Z = -1/e$, and thus given by

$$U_{\max} = \ln\left[-\frac{1+\ln(a)}{b}\right] = \ln\left[\frac{1-k_0-k_0\ln\frac{1-\eta}{k_0}}{\eta}\right]. \tag{37}$$

For times up to peak time the solution (36) applies, using the non-principal branch of Lambert's function,

$$\tau = -\frac{1}{k_0}\int_0^{U} \frac{dx}{1+W_{-1}\left(\alpha e^{\frac{\eta e^x}{k_0}}\right)} \qquad (0 \le \tau \le \tau_U), \tag{38}$$

with the peak time τ_U determined by

$$\tau_U \quad = \quad -\frac{1}{k_0}\int_0^{U_{\max}} \frac{dx}{1+W_{-1}\left(\alpha e^{\frac{\eta e^x}{k_0}}\right)}. \tag{39}$$

Over this interval $U(\tau)$ monotonically increases from $U(0) = 0$ to $U(\tau_U) = U_{\max}$. Beyond peak time, the solution is determined by

$$\tau = \tau_U + \frac{1}{k_0}\int_U^{U_{\max}} \frac{dx}{1+W_0\left(\alpha e^{\frac{\eta e^x}{k_0}}\right)} \qquad (\tau \ge \tau_U). \tag{40}$$

Over this remaining interval $U(\tau)$ monotonically decreases towards $\lim_{\tau\to\infty} U(\tau) = -\infty$.

The respective slopes below and above the peak time are obtained by taking the derivative with respect to τ of Equations (38) and (40) providing

$$\frac{dU}{d\tau}(\tau \le \tau_U) = -k_0\left[1+W_{-1}\left(\alpha e^{\frac{\eta e^{U(\tau)}}{k_0}}\right)\right] \tag{41}$$

and

$$\frac{dU}{d\tau}(\tau \ge \tau_U) = -k_0\left[1+W_0\left(\alpha e^{\frac{\eta e^{U(\tau)}}{k_0}}\right)\right], \tag{42}$$

respectively. At very large times the latter approaches

$$\lim_{\tau\to\infty}\frac{dU}{d\tau} = -k_0[1+W_0(\alpha)], \tag{43}$$

since $\lim_{\tau\to\infty} U(\tau) = -\infty$.

 doi:10.20944/preprints202411.0521.v1

3.2. Resulting Fractions

Using the notation $W_s(Z)$ and $W'_s(Z) = dW_s(Z)/dZ$ with $s = -1$ for $\tau \leq \tau_U$ and $s = 0$ for $\tau \geq \tau_U$, respectively, and

$$Z = -\frac{1-\eta}{k_0} e^{\frac{\eta e^{U(\tau)}-1}{k_0}} = \alpha e^{\frac{\eta e^{U(\tau)}}{k_0}} = -\exp\left[\frac{\eta}{k_0}\left(e^{U(\tau)} - e^{U_{\max}}\right) - 1\right], \tag{44}$$

with negative α, the solutions Equations (41)–(42) read

$$\frac{dU}{d\tau} = -k_0[1 + W_s(Z)]. \tag{45}$$

Then, according to Equation (15) one finds

$$S(\tau) = U'(\tau) + k_0 = -k_0 W_s(Z) = -k_0 W_s\left(\alpha e^{\frac{\eta e^{U(\tau)}}{k_0}}\right), \tag{46}$$

so that with $Z_\infty = \alpha$

$$S_\infty = S(\tau = \infty) = -k_0 W_0(\alpha), \tag{47}$$

in agreement with the exact KSSIR result (A10a). Using

$$\frac{dZ}{d\tau} = \frac{\eta}{k_0}\frac{dU(\tau)}{d\tau} e^{U(\tau)} Z = -\eta Z e^{U(\tau)}[1 + W_s(Z)], \tag{48}$$

one obtains for the first derivative of Equation (46) with respect to τ

$$\frac{dS}{d\tau} = -k_0 \frac{dZ}{d\tau} W'_s(Z) = \eta k_0 Z e^{U(\tau)}[1 + W_s(Z)] W'_s(Z) = \eta k_0 e^{U(\tau)} W_s(Z), \tag{49}$$

where we used Lambert's equation (28). Inserting Equations (46) and (49) yields for Equation (11)

$$I(\tau) = -\frac{dS(\tau)/d\tau}{S(\tau)} = \eta e^{U(\tau)} = -\frac{d}{d\tau}\ln\left[U'(\tau) + k_0\right] = -\frac{U''(\tau)}{U'(\tau) + k_0}, \tag{50}$$

where we used Equation (19b), thus correctly reproducing the earlier Equation (13). Obviously, the fraction of infected persons peaks at τ_U, because of its dependence $\propto e^{U(\tau)}$, and its maximum value is given by

$$I_{\max} = \eta e^{U_{\max}} = 1 - k_0 - k_0 \ln\frac{1-\eta}{k_0} \tag{51}$$

Consequently, one finds for the rate of new infections (9)

$$j(\tau) = S(\tau) I(\tau) = -U''(\tau) = \eta(1-\eta) U(\tau) e^{-\eta \int_0^\tau dx\, e^{U(x)}}, \tag{52}$$

where in the last step we used Equation (19d), and the corresponding cumulative fraction of infected persons

$$J(\tau) = 1 - S(\tau) = 1 + k_0 W_s(Z) = 1 + k_0 W_s\left(\alpha e^{\frac{\eta e^{U(\tau)}}{k_0}}\right). \tag{53}$$

Likewise, the sum constraint (7d) leads to

$$R(\tau) = 1 - S(\tau) - \frac{j(\tau)}{1 - J(\tau)} = 1 - k_0 - U'(\tau) + \frac{U''(\tau)}{U'(\tau) + k_0} \tag{54}$$

 doi:10.20944/preprints202411.0521.v1

As $U(\infty) = -\infty$ we derive

$$I_\infty = j_\infty = 0, \tag{55a}$$
$$R_\infty = J_\infty = 1 - S_\infty = 1 + k_0 W_0(\alpha), \tag{55b}$$

reproducing exactly the earlier noted properties (A8) and (A10).

We thus have expressed all quantities of interest, the fractions S, I, R as well as the differential rate of new infections and its corresponding cumulative number in terms of the function $U(\tau)$ and its first and second derivatives. These expressions are exact. It remains to derive the direct reduced time dependence of the function $U(\tau)$ which is done approximately for large and small times in the following sections.

4. Approximated $U(\tau)$ for Large and Small Times

4.1. Large Times $\tau \geq \tau_U$

We note that the function $Z(\tau)$ in Equation (44) has values

$$-Z(\tau_U) = e^{-1}, \qquad -Z(\tau = \infty) = -\alpha = \frac{(1-\eta)e^{-\frac{1}{k_0}}}{k_0}, \tag{56}$$

so that $0 < |Z(\tau = \infty)| < |Z(\tau_U)| < e^{-1}$. For such small values of Z we then use as approximation

$$W_0(Z) \simeq (1 + eZ)^{1/2} - 1, \tag{57}$$

shown in Figure 1 in comparison to the exact variation. As can be seen the agreement is sufficient, and the approximation exact at the terminals.

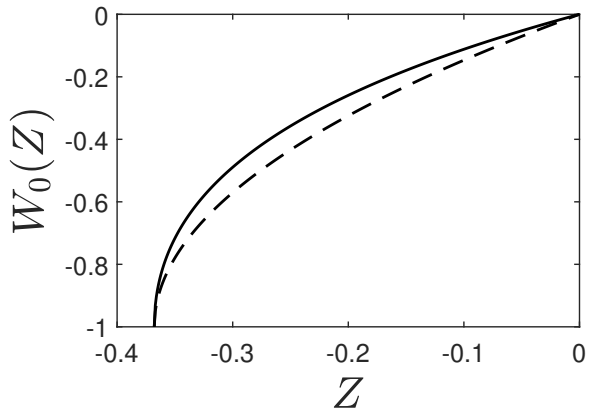

]

Figure 1. Principal branch of Lambert's function. Approximation (57) (dashed) for $W_0(Z)$ (solid).

The approximation (57) then yields for Equation (40)

$$k_0(\tau - \tau_U) \simeq \int_U^{U_{\max}} \frac{dx}{\sqrt{1 + \alpha e \exp(\eta e^x / k_0)}} = \int_{\frac{\eta e^U}{k_0}}^{\frac{\eta e^{U_{\max}}}{k_0}} \frac{dy}{y\sqrt{1 + \alpha e e^y}}, \tag{58}$$

where we substituted $y = \eta e^x / k_0$. The upper integration limit is given by

$$\mathcal{O}(k_0) = \frac{\eta e^{U_{\max}}}{k_0} = \frac{1}{k_0} - \left[1 + \ln\frac{1-\eta}{k_0}\right] \simeq \frac{1}{k_0} + \ln(k_0) - 1, \tag{59}$$

 doi:10.20944/preprints202411.0521.v1

where the second approximation holds for small values of $\eta \ll 1$. It is shown in Figure 2 as a function of k_0. The upper integration limit is thus smaller than unity provided $k_0(2 - \ln k_0) > 1$, corresponding to

$$k_0 > -W_{-1}(-e^{-2}) \approx 0.32 \tag{60}$$

in agreement with Figure 2.

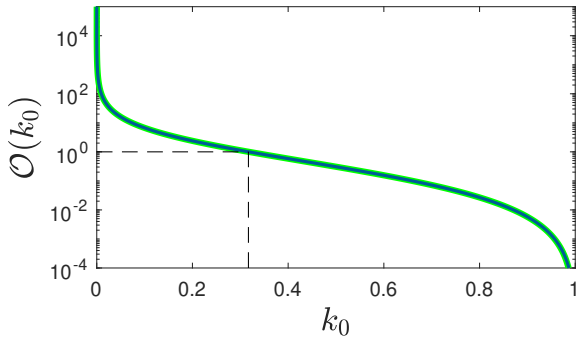

Figure 2. Upper bound $\mathcal{O}(k_0) = \eta e^{U_{\max}}/k_0$ versus k_0 for $\eta = 10^{-5}$. Shown is both the exact expression (black line) and the approximant (59) (green line). The dashed lines mark $\mathcal{O}(k_0) = 1$. The curve is basically unaltered for smaller η.

For such values of k_0 we approximate

$$1 + \alpha e e^y \simeq 1 + \alpha e + \alpha e y \tag{61}$$

to obtain with

$$\kappa = -\frac{\alpha e}{1 + \alpha e} = \left[\frac{k_0}{1-\eta} e^{\frac{1}{k_0}-1} - 1\right]^{-1} = \left[e^{\frac{\eta e^{U_{\max}}}{k_0}} - 1\right]^{-1} = \frac{1}{e^{\mathcal{O}(k_0)} - 1} \tag{62}$$

for the integral (58)

$$\sqrt{1+\alpha e}\, k_0(\tau - \tau_U) = \frac{k_0(\tau - \tau_U)}{\sqrt{1+\kappa}} \simeq \int_{\frac{\eta e^U}{k_0}}^{\frac{\eta e^{U_{\max}}}{k_0}} \frac{dy}{y\sqrt{1-\kappa y}} \tag{63}$$

With the substitution $s = 1 - \kappa y$ one finds for the last equation

$$\begin{aligned} \frac{k_0(\tau - \tau_U)}{\sqrt{1+\kappa}} &= \int_{1-\frac{\eta\kappa e^{U_{\max}}}{k_0}}^{1-\frac{\eta\kappa}{k_0}e^U} \frac{ds}{(1-s)\sqrt{s}} = 2\left[\tanh^{-1}\sqrt{s}\right]_{1-\frac{\eta\kappa e^{U_{\max}}}{k_0}}^{1-\frac{\eta\kappa}{k_0}e^U} \\ &= \left[\ln\frac{1+\sqrt{s}}{1-\sqrt{s}}\right]_{1-\frac{\eta\kappa e^{U_{\max}}}{k_0}}^{1-\frac{\eta\kappa}{k_0}e^U} \end{aligned} \tag{64}$$

After straightforward algebra Equation (64) leads to

$$\frac{\eta\kappa e^{U(\tau)}}{k_0} = 1 - \tanh^2\left[\frac{k_0(\tau-\tau_U)}{2\sqrt{1+\kappa}} + \Phi\right] = \cosh^{-2}\left[\frac{k_0(\tau-\tau_U)}{2\sqrt{1+\kappa}} + \Phi\right] \tag{65}$$

with the constant Φ defined by

$$\Phi = \frac{1}{2}\ln\frac{1+\sqrt{1-\frac{\eta\kappa e^{U_{\max}}}{k_0}}}{1-\sqrt{1-\frac{\eta\kappa e^{U_{\max}}}{k_0}}} = \tanh^{-1}\sqrt{1-\frac{\kappa\eta}{k_0}e^{U_{\max}}} \tag{66}$$

Preprints.org (www.preprints.org) | NOT PEER-REVIEWED | Posted: 7 November 2024 doi:10.20944/preprints202411.0521.v1

Equation (65) readily provides as approximation at large times

$$U(\tau \geq \tau_U) = U_H(\tau) = \ln \frac{k_0}{\eta\kappa} - 2 \ln \cosh \zeta(\tau), \tag{67}$$

$$\zeta(\tau) = \frac{k_0(\tau - \tau_U)}{2\sqrt{1+\kappa}} + \Phi. \tag{68}$$

We note that Equation (67) correctly provides $U_H(\tau_U) = U_{\max}$ as $\cosh(\zeta(\tau_U)) = \cosh \Phi = \sqrt{k_0/\eta\kappa e^{U_{\max}}}$.

The slope of the approximation (67) is

$$U'(\tau \geq \tau_U) = -\frac{k_0}{\sqrt{1+\kappa}} \tanh \zeta(\tau), \tag{69}$$

providing for its limiting slope

$$\lim_{\tau\to\infty} \frac{dU_H}{d\tau} = -\frac{k_0}{\sqrt{1+\kappa}} = \sqrt{k_0\left[k_0 - (1-\eta)e^{1-\frac{1}{k_0}}\right]}, \tag{70}$$

which Figure 3 compares favorably well with the exact limiting slope given by Equation (43).

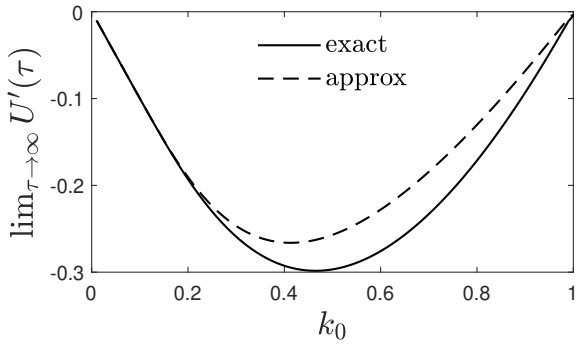

Figure 3. Limiting slope of $U(\tau)$. Exact numerical result using Equation (43) and approximation (70). Following [106] the numerical solution of the GSL equations we obtained using the 10th order predictor–corrector Adams method [107,108]. Within 0.1% precision, a single-step solver based on a modified Rosenbrock formula of order 2, implemented by [109] as ode23s in Matlab^{TM} yielded practically indistinguishable results.

It is tempting to use approximation (67) to calculate the corresponding $U'(\tau \geq \tau_U)$ as in Equation (69) and $U''(\tau \geq \tau_U)$ to infer directly the three fractions S, I and R as well as the differential rate j at large times. However, this produces incorrect results as can be seen with the resulting

$$S(\tau \geq \tau_U) = U'(\tau \geq \tau_U) + k_0 = k_0[1 - \frac{\tanh \zeta(\tau)}{\sqrt{1+\kappa}}] \tag{71}$$

implying

$$S_\infty = k_0\left(1 - \frac{1}{\sqrt{1+\kappa}}\right) = k_0\left(1 - \sqrt{1 - \frac{1-\eta}{k_0}e^{1-\frac{1}{k_0}}}\right) \simeq \frac{1-\eta}{2k_0}e^{1-\frac{1}{k_0}} \tag{72}$$

which is finite but slightly disagrees with the exact final value (47), as shown in Figure 4.

 doi:10.20944/preprints202411.0521.v1

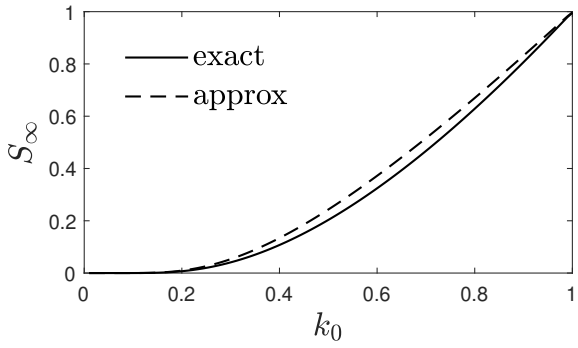

Figure 4. Limiting susceptible fraction. Exact (47) and approximate (72) analytic expressions for S_∞. For this plot, $\eta = 10^{-5}$, but the situation is very comparable for any $\eta \ll 1$.

The proper way to continue is to only use Equation (67) as an approximation for $U(\tau \geq \tau_U)$ and to insert it in the earlier general expressions for the fractions. With this approximation we obtain for Equation (44)

$$Z(\tau \geq \tau_U) = \alpha \exp\left(\frac{1}{\kappa \cosh^2 \zeta(\tau)}\right), \tag{73a}$$

$$Z(\tau_U) = \alpha \exp\left(\frac{\eta e^{U_{\max}}}{k_0}\right) = -\frac{1}{e}, \tag{73b}$$

and consequently for the fraction (46)

$$\begin{aligned} S(\tau \geq \tau_U) &= 1 - J(\tau \geq \tau_U) = -k_0 W_0(Z(\tau \geq \tau_U)) \\ &= -k_0 W_0\left[\alpha \exp\left(\frac{1}{\kappa \cosh^2 \zeta(\tau)}\right)\right], \end{aligned} \tag{74}$$

which in contrast to the incorrect Equation (72) now correctly approaches $S_\infty = -k_0 W_0(\alpha)$. For later use we note

$$S(\tau_U) = -k_0 W_0(-e^{-1}) = k_0 \tag{75}$$

Likewise, the fraction (50) at large times is given by

$$I(\tau \geq \tau_U) = k_0 \ln \frac{Z}{\alpha} = \frac{k_0}{\kappa \cosh^2 \zeta(\tau)}, \tag{76}$$

reproducing correctly $I_\infty = 0$. The rate of new infections (9) then is

$$\begin{aligned} j(\tau \geq \tau_U) &= S(\tau \geq \tau_U) I(\tau \geq \tau_U) = -\frac{k_0^2 W_0\left[\alpha \exp\left(\frac{1}{\kappa \cosh^2 \zeta(\tau)}\right)\right]}{\kappa \cosh^2 \zeta(\tau)} \\ &= -k_0^2 W_0(Z) \ln \frac{Z}{\alpha}. \end{aligned} \tag{77}$$

Preprints.org (www.preprints.org) | NOT PEER-REVIEWED | Posted: 7 November 2024 doi:10.20944/preprints202411.0521.v1

4.2. Small Times $\tau \leq \tau_U$

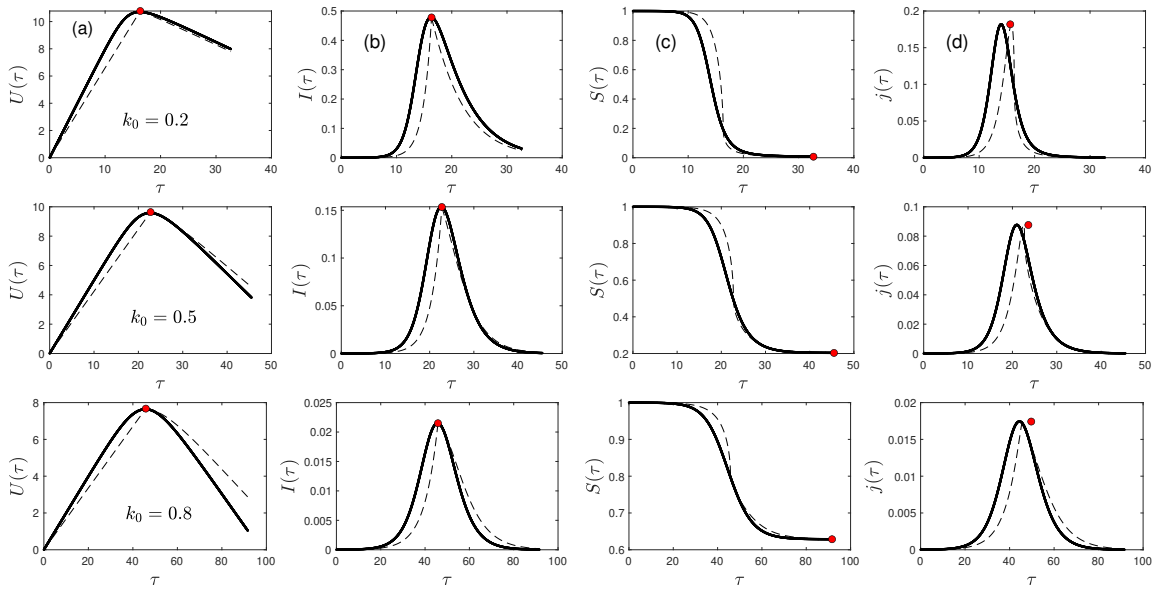

Figure 5. Time evolution of the functions $U(\tau)$, $I(\tau)$, $S(\tau)$, and $j(\tau)$. (a) Numerical $U(\tau)$ from (14) (solid) compared with $U(\tau)$ from (67) and (85) (dashed), using ζ from Equation (68), Φ from Equation (66), ρ from (82), κ from (62), τ_U from (39), $U_{\max}$ from (37). The red bullet marks $(\tau_U, U_{\max})$. (b) Numerical $I(\tau)$ (solid) compared with $I(\tau)$ from Equations (76) and (88). The red bullet marks $(\tau_I = \tau_U, I_{\max})$ from Equations (39) and (51). (c) Numerical $S(\tau)$ (solid) compared with $S(\tau)$ from Equations (87) and (74). The red bullet marks S_∞ (47). (d) Numerical $j(\tau)$ (solid) compared with $j(\tau)$ from Equations (93) with Z_s according to Equation (94). The red filled bullet marks $(\tau_j, j_{\max})$ according to Equations (103) and (106). Parameters: $\eta = 10^{-5}$ and $k_0 \in \{0.2, 0.5, 0.8\}$ mentioned in the left panel.

For small times where $U(\tau) \ll 1$ we expand the double-exponential function on the right-hand side of Equation (19c) to first order as

$$\begin{aligned} e^{-\eta \int_0^\tau dx\, e^{U(x)}} &\simeq 1 - \eta \int_0^\tau dx\, e^{U(x)} \simeq 1 - \eta \int_0^\tau dx\, [1 + U(x)] \\ &= 1 - \eta\tau - \eta \int_0^\tau dx\, U(x), \end{aligned} \tag{78}$$

so that Equation (19c) becomes

$$\frac{dU(\tau)}{d\tau} + \eta(1-\eta)\left[\tau + \int_0^\tau dx\, U(x)\right] \simeq 1 - \eta - k_0, \tag{79}$$

fulfilling the correct initial condition $U'(0) = 1 - \eta - k_0$. Setting

$$\int_0^\tau dx\, U(x) = F(\tau) - \tau + \frac{1 - \eta - k_0}{\eta(1-\eta)}, \tag{80}$$

Equation (79) reduces to

$$\frac{d^2F(\tau)}{d\tau^2} + \eta(1-\eta)F(\tau) = 0, \tag{81}$$

with the solution

$$F(\tau) = C_1 \sin(\rho\tau) + C_2 \cos(\rho\tau), \qquad \rho = \sqrt{\eta(1-\eta)}. \tag{82}$$

 doi:10.20944/preprints202411.0521.v1

Therefore

$$\begin{aligned} \int_0^\tau dx\, U(x) &= C_1 \sin(\rho\tau) + C_2 \cos(\rho\tau) - \tau + \frac{1-\eta-k_0}{\eta(1-\eta)}, \\ U(\tau) &= \rho[C_1 \cos(\rho\tau) - C_2 \sin(\rho\tau)] - 1. \end{aligned} \tag{83}$$

The two integration constants C_1 and C_2 are determined by the conditions $U(0) = 0$ and $U(\tau_U) = U_{\max}$ yielding

$$C_1 = \frac{1}{\rho}, \qquad C_2 = \frac{\cos(\rho\tau_U) - 1 - U_{\max}}{\rho \sin(\rho\tau_U)}. \tag{84}$$

Consequently

$$U(\tau \le \tau_U) = U_L(\tau) = g(\tau) - 1, \tag{85a}$$

$$g(\tau) = \frac{\sin\rho(\tau_U - \tau) + (1 + U_{\max})\sin(\rho\tau)}{\sin(\rho\tau_U)}. \tag{85b}$$

Since $U(\tau_U) = U_{\max}$ guarantees, according to Equations (44) and (46), that $Z(\tau_U) = -e^{-1}$ implying $W_{-1}(Z(\tau_U)) = -1$, with the approximation (85) also $S(\tau_U) = k_0$ is in agreement with Equation (75).

For general small times Equation (44) subjected to the approximation Equation (85a) provides

$$Z(\tau \le \tau_U) = \alpha e^{\frac{\eta}{k_0} e^{g(\tau)-1}}, \tag{86}$$

so that Equation (46) leads to

$$S(\tau \le \tau_U) = 1 - J(\tau \le \tau_U) = -k_0 W_{-1}\left(\alpha e^{\frac{\eta}{k_0} e^{g(\tau)-1}}\right). \tag{87}$$

Likewise, the fraction (50) at small times is given by

$$I(\tau \le \tau_U) = \eta e^{g(\tau)-1}, \tag{88}$$

reproducing correctly $I(\tau = 0) = \eta$. The rate of new infections (9) then is

$$j(\tau \le \tau_U) = S(\tau \le \tau_U) I(\tau \le \tau_U) = -\eta k_0 e^{g(\tau)-1} W_{-1}\left(\alpha e^{\frac{\eta}{k_0} e^{g(\tau)-1}}\right). \tag{89}$$

We recall that Equation (39) determines

$$\tau_U = -\frac{1}{k_0} \int_0^{U_{\max}} \frac{dx}{1 + W_{-1}\left(\alpha e^{\frac{\eta e^x}{k_0}}\right)}. \tag{90}$$

so that for given values η and k_0 all parameters are fixed.

In most applications the initial fraction of infected persons $\eta \simeq \mathcal{O}(10^{-5})$ is very small. Hence for reduced times $\tau \le \tau_U \ll \eta^{-1/2}$ one can further approximate

$$\sin(\rho\tau) \simeq \rho\tau, \qquad \sin(\rho\tau_U) \simeq \rho\tau_U, \qquad \sin[\rho(\tau_U - \tau)] \simeq \rho(\tau_U - \tau) \tag{91}$$

to obtain for the function (85b)

$$g(\tau \le \tau_U) \simeq 1 + \frac{\tau}{\tau_U} U_{\max}, \tag{92}$$

i.e., one may replace $g(\tau) - 1$ in Equations (86)–(89) by $\tau U_{\max}/\tau_U$ with $U_{\max}$ from Equation (37).

Preprints.org (www.preprints.org) | NOT PEER-REVIEWED | Posted: 7 November 2024 doi:10.20944/preprints202411.0521.v1

5. Results

5.1. Rate of New Infections

According to Equations (77) and (89) with our earlier notation the rate of new infections at all reduced times is given by

$$j(\tau) = -k_0^2 W_s(Z_s) \ln \frac{Z_s}{\alpha} \tag{93}$$

with

$$Z_{-1} = Z_L = \alpha e^{\frac{\eta}{k_0} e^{g(\tau)-1}}, \quad \tau \leq \tau_U \tag{94a}$$

$$Z_0 = Z_H = \alpha e^{\kappa^{-1} \cosh^{-2} \zeta(\tau)}, \quad \tau \geq \tau_U \tag{94b}$$

We note that

$$\frac{Z_L}{\alpha} \in [e^{\frac{\eta}{k_0}}, e^{\mathcal{O}(k_0)}] \geq 1, \tag{95a}$$

$$\frac{Z_H}{\alpha} \in [1, e^{\mathcal{O}(k_0)}] > 1. \tag{95b}$$

In the last column of Figure 5 we compare this rate of new infections based on τ_U from Equation (90) with the exact numerical solution for $\eta = 10^{-5}$ and several choices of the parameter $k_0 = 0.2, 0.5, 0.8$. One notices excellent agreement between the analytical and numerical curves in all three cases.

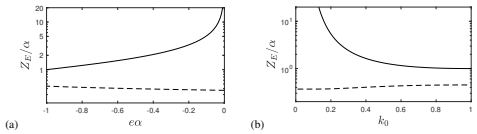

Figure 6. Extremum of $Z(\tau)$. Z_E/α (102) versus (a) $e\alpha$ and (b) k_0. Shown are the cases of $s = -1$ (solid) and $s = 0$ (dashed). For this plot $\eta = 10^{-5}$, but the plots are basically unaffected by η for $\eta \ll 1$.

The rate of new infections (93) attains its maximum for a vanishing first derivative

$$\begin{aligned}
\frac{dj(\tau)}{d\tau} &= -k_0^2 \frac{dZ_s}{d\tau} \frac{d}{dZ_s} [W_s(Z_s) \ln \frac{Z_s}{\alpha}] \\
&= \eta k_0^2 Z_s e^{U_s} [1 + W_s(Z_s)] \left[W_s'(Z_s) \ln \frac{Z_s}{\alpha} + \frac{W_s(Z_s)}{Z_s} \right] \\
&= \eta k_0^2 e^{U_s} W_s(Z_s) [1 + W_s(Z_s)] \left[1 + \frac{Z_s W_s'(Z_s)}{W_0(Z_s)} \ln \frac{Z_s}{\alpha} \right] \\
&= \eta k_0^2 e^{U_s} W_s(Z_s) \left[1 + W_s(Z_s) + \ln \frac{Z_s}{\alpha} \right] = 0,
\end{aligned} \tag{96}$$

where we used Equations (48) and (28). Thus the maximum occurs at Z_E given by the solution of

$$1 + W_s(Z_E) + \ln \frac{Z_E}{\alpha} = 0. \tag{97}$$

Taking the exponential of the last equation leads to

$$\frac{\alpha}{e} = Z_E e^{W_s(Z_E)} = W_s(Z_E) e^{2W_s(Z_E)}, \tag{98}$$

 doi:10.20944/preprints202411.0521.v1

where we used Equation (24). Setting $X = 2W_s(Z_E)$ one can cast Equation (98) into the form

$$e^{-X} = \frac{e}{2\alpha} X \tag{99}$$

with the solution

$$X = W_s\left(\frac{2\alpha}{e}\right) \tag{100}$$

and consequently

$$W_s(Z_E) = \frac{1}{2} W_s(\alpha_0), \qquad \alpha_0 = \frac{2\alpha}{e}, \tag{101}$$

where we introduced α_0. Applying Equation (34) then provides

$$Z_E = \frac{1}{2} W_s(\alpha_0) e^{\frac{1}{2}W_s(\alpha_0)} = -\frac{1}{2}\sqrt{\alpha_0 W_s(\alpha_0)}, \tag{102}$$

where Equation (24) and $\sqrt{-a} = \imath\sqrt{a}$ for positive values $a > 0$ has been used. The maximum is then given by

$$\begin{aligned} j_{\max} &= k_0^2 W_s(Z_E)[1 + W_s(Z_E)] = \frac{k_0^2}{4} W_s(\alpha_0)[2 + W_s(\alpha_0)] \\ &= \frac{k_0^2}{4}\Big\{[1 + W_s(\alpha_0)]^2 - 1\Big\}, \end{aligned} \tag{103}$$

where we inserted Equation (101). Equation (103) agrees exactly with the well-known KSSIR expression (A14) only if $s = -1$, i.e., only if the non-principal branch of the Lambert functions $W_{-1}(\alpha_0)$ in the solution (102) is chosen. The second solution $Z_E = -0.5\sqrt{\alpha_0 W_s(\alpha_0)}$ involving the principal branch $W_0(\alpha_0)$ can be ruled out as it provides values of $Z_E/\alpha = Z_H/\alpha$ smaller than unity, as can be seen by the dashed curves in Figure 6 that reside clearly outside of the possible values of Z_H/α according to Equation (95b).

In Figure 6 we calculate from Equation (102) Z_E/α as a function of k_0 for $\eta = 10^{-5}$. It can be seen that Z_E/α is always greater than unity. Because of the property (95a) this indicates that the peak time of the rate of new infections $\tau_j < \tau_U$ occurs at times smaller than τ_U and is given by the solution of the Equation

$$e^{\frac{\eta}{k_0} e^{g(\tau_j)-1}} = \frac{W_{-1}(\alpha_0)}{2\alpha} = \frac{\alpha_0 e^{-W_{-1}(\alpha_0)}}{2\alpha} = e^{-[1+W_{-1}(\alpha_0)]}, \tag{104}$$

where we used Equation (24), so that

$$g(\tau_j) - 1 = \ln\left[\frac{k_0}{\eta}\ln\big(-[1 + W_{-1}(\alpha_0)]\big)\right] \tag{105}$$

With the approximation (92) one obtains

$$\tau_j = \frac{\tau_U}{U_{\max}} \ln\left[\frac{k_0}{\eta}\ln\big(-[1 + W_{-1}(\alpha_0)]\big)\right]. \tag{106}$$

In Figure 7 the ratio τ_j/τ_I is displayed as a function of k_0 for $\eta = 10^{-5}$. The ratio always is smaller than unity demonstrating that the rate of new infections peaks before the fraction of infected persons in agreement also with the second and fourth columns in Figure 5.

 doi:10.20944/preprints202411.0521.v1

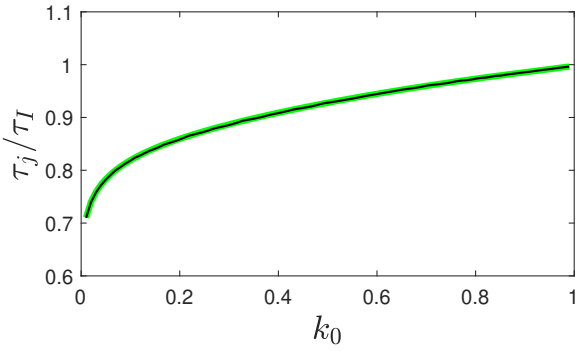

Figure 7. Ratio of peak times . Numerical $\tau_j/\tau_I = \tau_j/\tau_U$ (solid black) compared with this ratio using the analytical expression Equation (A15) with J_0 from Equation (A13) (thick green), which is well approximated by the simpler Equations (93) and (39) with Z_s according to Equation (94). For this figure, $\eta = 10^{-5}$.

5.2. Peak Time of Fraction of Infected Persons

The peak time τ_I of the fraction of infected persons is of particular interest [70,75,89,110–120]. According to Equation (50) this peak time τ_I coincides with τ_U given exactly by Equation (39). Consequently, we can compare this exact peak time with approximants derived before [103]. Figure 8 demonstrates in the first column that the analytical equation (39) coincides with the numerically calculated peak time τ_I. While the earlier SK-I approximant (shown in the third column) provides acceptable agreement in a wide range of parameter values, the MT-approximant (shown in the second column) is less accurate.

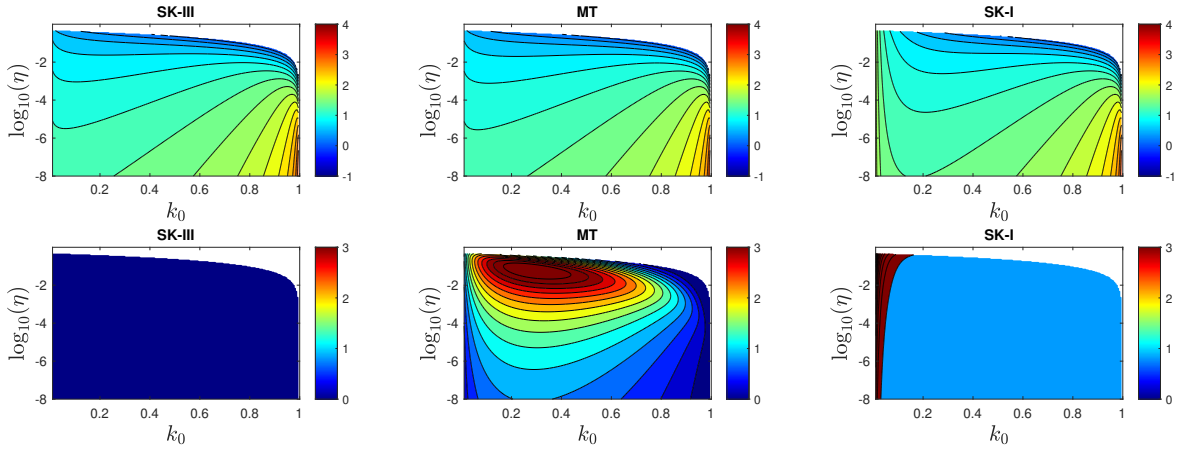

Figure 8. Comparison of analytical approximants for τ_I. The top row shows the decadic logarithm of τ_I (colormap) versus k_0 and η for $k_0 \leq 1 - 2\eta$, while the 2nd row shows the relative deviation (in %) between the exact τ_I and the approximant. The first column displays the analytical τ_I (39) (here denoted as SL-III), which coincides with the exact result, the second column the so-called MT-approximant proposed in Ref. [103], and the third column the SK-I-approximant [103].

6. Summary and Conclusions

We have derived a near-exact analytical solution of the statistical Susceptible-Infectious-Recovered (SIR) epidemics model for a constant ratio k_0 (referred to as KSSIR case) of infection ($a(t)$) to recovery ($\mu(t)$) rates in the semi-time case which is particularly appropriate for modeling the temporal evolution of later (than the first) pandemic waves when a greater population fraction from the first wave has been infected. By introducing the dimensionless reduced time variable $\tau = \int_{t_0}^{t} d\xi\, a(\xi)$ the derived solution holds for stationary rates as well as for the case of the same real time-dependency of the recovery and infection rates. The accuracy of the analytical solutions is confirmed by comparison with

 doi:10.20944/preprints202411.0521.v1

the exact numerical solutions of the SIR equations. Exact as well as accurately approximative solutions serve dual important purposes: first, they are suitable benchmarks for numerical codes, and secondly, they allow us to understand the fundamental behavior and functional patterns of epidemic outbursts as well as the decisive role of parameters.

The newly developed KSSIR-solution is not of inverse form as the known KSSIR solutions in the literature but rather directly expresses the three fractions $S(\tau)$, $I(\tau)$ and $R(\tau)$ and thus the rate of new infections $j(\tau) = S(\tau)I(\tau)$ exactly in terms of the same function $U(\tau) = -k_0\tau + \int_0^\tau dx\, S(x)$. With respect to the reduced time these fractions depend on two parameters: predominantly on the ratio k_0 and only weakly on the usually very small initial fraction η of infected persons. With respect to real time additionally the predescribed time dependent infection rate $a(t)$ enters via the reduced time. These exact expressions involve the principal and non-principal branches of the Lambert functions, which routinely are available in mathematical software packages such as Python (scipy), Excel, Matlab and Mathematica, above and below the peak time of the function $U(\tau)$ which agrees with the peak time of the rate of infections $I(\tau)$. The newly developed solution correctly reproduces all known exact expressions of the earlier KSSIR solution including the final values of S_∞, I_∞, and R_∞. It also provides exact analytical formulas for the peak time $\tau_I = \tau_U$ and the maximum fraction $I_{\max}$. These allow to check the accuracy of earlier derived approximants for τ_I. In particular it is shown that the rate of new infections peaks before the fraction of infected persons.

The derived near-exact solution is not entirely exact because the reduced time dependence of $U(\tau)$ obeying a nonlinear integro-differential equation is only obtained approximately for small and large times with respect to τ_U. At small reduced times where $U(\tau) \ll 1$ the approximation is based on the expansion of a double-exponential function to first-order, whereas at large reduced times an accurate simple approximation of the principal Lambert function $W_0(Z)$ is employed. The resulting rate of new infections correctly reproduces the known exact maximum rate of new infections.

Author Contributions: R.S.: conceptualization, methodology, formal analysis, writing-reviewing and editing; M.K.: methodology, formal analysis, software, writing-reviewing and editing, visualization. All authors have read and agreed to the published version of the manuscript.

Funding: This research received no external funding.

Informed Consent Statement: Not applicable.

Data Availability Statement: All data are enclosed with this publication.

Conflicts of Interest: The authors declare no conflict of interest

Appendix A. Inverse KSSIR-Solution of Earlier Work

For stationary ratios (18) Equation (7c) immediately integrates to

$$R(\tau) = -k_0 \ln \frac{S(\tau)}{1-\eta} = -k_0 \ln\left[\frac{1-J(\tau)}{1-\eta}\right], \tag{A1}$$

where we used $S(\tau) = 1 - J(\tau)$ from Equation (10) so that also

$$I(\tau) = -\frac{d\ln[1-J(\tau)]}{d\tau} \tag{A2}$$

With these expressions the sum constraint (7c) then reads

$$J(\tau) + \frac{d\ln[1-J(\tau)]}{d\tau} + k_0 \ln\left[\frac{1-J(\tau)}{1-\eta}\right] = 0, \tag{A3}$$

implying

$$\frac{dJ(\tau)}{d\tau} = [1-J(\tau)]\left[J(\tau) + k_0 \ln\frac{1-J(\tau)}{1-\eta}\right] \tag{A4}$$

 doi:10.20944/preprints202411.0521.v1

With the initial condition $J(0) = \eta$ Equation (A4) readily is solved in inverse form as

$$\tau = \int_{\eta}^{J} \frac{dx}{(1-x)[x + k_0 \ln \frac{1-x}{1-\eta}]}. \tag{A5}$$

This solution (A5) generalizes the known analytical solutions in the literature [1,2,121] as it holds for arbitrary time-dependence of the infection rate $a(t)$. The mentioned known solutions can be reproduced with Equation (A5) by setting $\tau = a_0 t$ on its left-hand side resulting from a constant injection rate a_0.

Taking the derivative with respect to τ highlights the fact that the inverse integrand in (A5) is nothing but the differential rate of newly infected persons in terms of $J(\tau)$, i.e.,

$$j(\tau) \quad = \quad (1 - J(\tau)) \left[J(\tau) + k_0 \ln \frac{1 - J(\tau)}{1 - \eta} \right]. \tag{A6}$$

It has been noted before that important exact properties of the KSSIR-solution (A5) can be inferred without doing the inversion to $J(\tau)$.

Appendix A.1. Final and Maximum Values

The solution (A5) indicates that the maximum value $J_\infty = J(\tau = \infty)$ is attained when the denominator of the respective integrand vanishes, i.e.,

$$J_\infty + k_0 \ln \left(\frac{1 - J_\infty}{1 - \eta} \right) = 0. \tag{A7}$$

Consequently,

$$J_\infty = 1 + k_0 W_0(\alpha), \tag{A8}$$

where W_0 is the principal solution of Lambert's equation and

$$\alpha = -\frac{(1-\eta)e^{-1/k_0}}{k_0}. \tag{A9}$$

The knowledge of J_∞ from Equation (A8) immediately yield

$$S_\infty \quad = \quad 1 - J_\infty = -k_0 W_0(\alpha), \tag{A10a}$$

$$R_\infty \quad = \quad -k_0 \ln \frac{1 - J_\infty}{1 - \eta} = J_\infty, \tag{A10b}$$

$$I_\infty \quad = \quad 1 - S_\infty - R_\infty = 0,, \tag{A10c}$$

$$j_\infty \quad = \quad j(\tau = \infty) = 0. \tag{A10d}$$

Appendix A.2. Peak Differential Rate

Likewise, the maximum of the differential rate (A6) occurs when the derivative $(dj/dJ)_{J_0} = 0$ vanishes. With Equation (A6) one finds

$$\frac{dj}{dJ} = 1 - 2J - k_0[1 - \ln(1-\eta)] - k_0 \ln(1 - J), \tag{A11}$$

yielding for J_0 the transcendental equation

$$2J_0 = 1 - k_0 + k_0 \ln(1-\eta) - k_0 \ln(1 - J_0), \tag{A12}$$

 doi:10.20944/preprints202411.0521.v1

which is solved in terms of the non-principal Lambert function as

$$J_0 = 1 + \frac{k_0}{2} W_{-1}(\alpha_0), \qquad \alpha_0 = \frac{2\alpha}{e}, \tag{A13}$$

with α from (A9). Inserting Equation (A13) in Equation (A6) and making use of Equation (A12) yields for the maximum value in reduced time

$$j_{\max} = j(J_0) = (1 - J_0)(1 - J_0 - k_0) = \frac{k_0^2}{4}\Big\{[1 + W_{-1}(\alpha_0)]^2 - 1\Big\} \tag{A14}$$

According to Equation (A5) the peak time of the differential rate (A6) is given by

$$\tau_j = \int_\eta^{J_0} \frac{dx}{(1-x)[x + k_0 \ln \frac{1-x}{1-\eta}]}. \tag{A15}$$

For a maximum to occur at finite positive times $\tau_j > 0$, the derivative $dj/d\tau$ has to be positive at times $0 \le \tau < \tau_j$. With Equations (A11) - (A12) we readily find

$$\begin{aligned} \frac{dj}{d\tau} &= \frac{dJ}{d\tau}\frac{dj}{dJ} = j\frac{dj}{dJ} = j(\tau)[1 - 2J(\tau) - k_0(1 - \ln(1-\eta)) - k_0 \ln(1 - J(\tau))] \\ &= j(\tau)\left[2(J_0 - J(\tau)) - k_0 \ln \frac{1 - J(\tau)}{1 - J_0}\right]. \end{aligned} \tag{A16}$$

Since the requirement of a maximum $j_{\max}$ to exist at positive times is identical to the requirement of a positive $dj/d\tau$ at $\tau = 0$, we can insert $J(0) = \eta$ into the last equality in the first line of Equation (A16) to find

$$\left.\frac{dj}{d\tau}\right|_{\tau=0} = \eta(1-\eta)[1 - 2\eta - k_0] > 0 \tag{A17}$$

implying

$$k_0 < 1 - 2\eta. \tag{A18}$$

For inverse reproduction numbers k_0 greater than $1 - 2\eta$, the daily rate is monotonically decreasing at all times from its initial value $j(0) = \eta(1 - \eta)$ (decay phase). Contrary, for $k_0 < 1 - 2\eta$ the daily rate of newly infected persons attains a maximum at a finite positive time (peak case). At $k_0 = 1 - 2\eta$ the daily rate starts in its maximum at $\tau = 0$, and then decreases, while S, R and J approach their final values below unity.

References

1. Kermack, W.O.; McKendrick, A.G. A contribution to the mathematical theory of epidemics. *Proc. Royal Soc. A* **1927**, *115*, 700–721.
2. Kendall, D.G. Deterministic and stochastic epidemics in closed populations. In *Proc. Third Berkeley Symp. on Math. Statist. and Prob.*; Univ. of Calif. Press, Berkeley, United States, 1956; Vol. 4, pp. 149–165.
3. Babajanyan, S.G.; Cheong, K.H. Age-structured SIR model and resource growth dynamics: a Covid-19 study. *Nonlinear Dynamics* **2021**, *104*, 2853–2864.
4. Turkyilmazoglu, M. Explicit formulae for the peak time of an epidemic from the SIR model. *Physica D-nonlinear Phenomena* **2021**, *422*, 132902.
5. Telles, C.R.; Lopes, H.; Franco, D. SARS-COV-2: SIR Model Limitations and Predictive Constraints. *Symmetry-basel* **2021**, *13*, 676.
6. Carvalho, A.M.; Goncalves, S. An analytical solution for the Kermack-McKendrick model. *Physica A* **2021**, *566*, 125659.

 doi:10.20944/preprints202411.0521.v1

7. Priesemann, V.; Brinkmann, M.M.; Ciesek, S.; Cuschieri, S.; Czypionka, T.; Giordano, G.; Gurdasani, D.; Hanson, C.; Hens, N.; Iftekhar, E.; Kelly-Irving, M.; Klimek, P.; Kretzschmar, M.; Peichl, A.; Perc, M.; Sannino, F.; Schernhammer, E.; Schmidt, A.; Staines, A.; Szczurek, E. Calling for pan-European commitment for rapid and sustained reduction in Sars-Cov-2 infections. *Lancet* **2021**, *397*, 92–93.
8. Mungkasi, S. Variational iteration and successive approximation methods for a SIR epidemic model with constant vaccination strategy. *Applied Mathematical Modelling* **2021**, *90*, 1–10.
9. dos Santos, I.F.F.; Almeida, G.M.A.; de Moura, F.A.B.F. Adaptive SIR model for propagation of Sars-Cov-2 in Brazil. *Physica A* **2021**, *569*, 125773.
10. Ghaffar, A.; Alanazi, S.; Alruwaili, M.; Sattar, M.U.; Ali, W.; Humayun, M.; Siddiqui, S.Y.; Ahmad, F.; Khan, M.A. Multi-Stage Intelligent Smart Lockdown using SIR Model to Control Covid 19. *Intelligent Automation And Soft Computing* **2021**, *28*, 429–445.
11. Law, K.B.; Peariasamy, K.M.; Gill, B.S.; Singh, S.; Sundram, B.M.; Rajendran, K.; Dass, S.C.; Lee, Y.L.; Goh, P.P.; Ibrahim, H.; Abdullah, N.H. Tracking the early depleting transmission dynamics of Covid-19 with a time-varying SIR model. *Scientific Reports* **2020**, *10*, 21721.
12. Brugnano, L.; Iavernaro, F.; Zanzottera, P. A multiregional extension of the SIR model, with application to the Covid-19 spread in Italy. *Mathematical Methods In The Applied Sciences* **2021**, *44*, 4414–4427.
13. Venkatasen, M.; Mathivanan, S.K.; Jayagopal, P.; Mani, P.; Rajendran, S.; Subramaniam, U.; Ramalingam, A.C.; Rajasekaran, V.A.; Indirajithu, A.; Sorakaya Somanathan, M. Forecasting of the Sars-Cov-2 epidemic in India using SIR model, flatten curve and herd immunity. *Journal of Ambient Intelligence And Humanized Computing* **2020**.
14. Heng, K.; Althaus, C.L. The approximately universal shapes of epidemic curves in the Susceptible-Exposed-Infectious-Recovered (SEIR) model. *Scientific Reports* **2020**, *10*, 19365.
15. Chekroun, A.; Kuniya, T. Global threshold dynamics of aninfection age-structured SIR epidemic model with diffusion under the Dirichlet boundary condition. *Journal of Differential Equations* **2020**, *269*, 117–148.
16. Cadoni, M.; Gaeta, G. Size and timescale of epidemics in the SIR framework. *Physica D-nonlinear Phenomena* **2020**, *411*, 132626.
17. Chen, Y.C.; Lu, P.E.; Chang, C.S.; Liu, T.H. A Time-Dependent SIR Model for Covid-19 With Undetectable Infected Persons. *Ieee Transactions On Network Science And Engineering* **2020**, *7*, 3279–3294.
18. Cooper, I.; Mondal, A.; Antonopoulos, C.G. A SIR model assumption for the spread of Covid-19 in different communities. *Chaos Solitons Fract.* **2020**, *139*, 110057.
19. Karaji, P.T.; Nyamoradi, N. Analysis of a fractional SIR model with General incidence function. *Appl. Math. Lett.* **2020**, *108*, 106499.
20. McMahon, A.; Robb, N.C. Reinfection with Sars-Cov-2: Discrete SIR (Susceptible, Infected, Recovered) Modeling Using Empirical Infection Data. *Jmir Public Health And Surveillance* **2020**, *6*, 279–287.
21. Chen, X.; Li, J.; Xiao, C.; Yang, P. Numerical solution and parameter estimation for uncertain SIR model with application to Covid-19. *Fuzzy Optimization And Decision Making* **2021**, *20*, 189–208.
22. Ahmetolan, S.; Bilge, A.H.; Demirci, A.; Peker-Dobie, A.; Ergonul, O. What Can We Estimate From Fatality and Infectious Case Data Using the Susceptible-Infected-Removed (SIR) Model? A Case Study of Covid-19. *Front. Med.* **2020**, *7*, 556366.
23. Gopagoni, D.; Lakshmi, P., V. Susceptible, Infectious and Recovered (SIR Model) Predictive Model to Understand the Key Factors of Covid-19 Transmission. *International Journal of Advanced Computer Science And Applications* **2020**, *11*, 296–302.
24. Sene, N. SIR epidemic model with Mittag?Leffler fractional derivative. *Chaos Solitons Fract.* **2020**, *137*, 109833.
25. Mohamadou, Y.; Halidou, A.; Kapen, P.T. A review of mathematical modeling, artificial intelligence and datasets used in the study, prediction and management of Covid-19. *Applied Intelligence* **2020**, *50*, 3913–3925.
26. Barlow, N.S.; Weinstein, S.J. Accurate closed-form solution of the SIR epidemic model. *Physica D-nonlinear Phenomena* **2020**, *408*, 132540.
27. Simon, M. SIR epidemics with stochastic infectious periods. *Stochastic Processes And Their Applications* **2020**, *130*, 4252–4274.
28. Postnikov, E.B. Estimation of Covid-19 dynamics "on a back-of-envelope?: Does the simplest SIR model provide quantitative parameters and predictions? *Chaos Solitons Fract.* **2020**, *135*, 109841.

29. Shah, S.T.A.; Mansoor, M.; Mirza, A.F.; Dilshad, M.; Khan, M.I.; Farwa, R.; Khan, M.A.; Bilal, M.; Iqbal, H.M.N. Predicting Covid-19 Spread in Pakistan using the SIR Model. *Journal of Pure And Applied Microbiology* **2020**, *14*, 1423–1430.
30. Zhao, X.; He, X.; Feng, T.; Qiu, Z. A stochastic switched SIRS epidemic model with nonlinear incidence and vaccination: Stationary distribution and extinction. *International Journal of Biomathematics* **2020**, *13*, 2050020.
31. Richard, N.A.; Robert, D.; Valentin, D.; Emma, H.B.; Jan, A. Potential impact of seasonal forcing on a Sars-Cov-2 pandemic. *Swiss Medical Weekly* **2020**, *150*, w20224.
32. Colombo, R.M.; Garavello, M. Optimizing vaccination strategies in an age structured SIR model. *Mathematical Biosciences And Engineering* **2020**, *17*, 1074–1089.
33. Samanta, S.; Sahoo, B.; Das, B. Dynamics of an epidemic system with prey herd behavior and alternative resource to predator. *Journal of Physics A* **2019**, *52*, 425601.
34. El Koufi, A.; Adnani, J.; Bennar, A.; Yousfi, . Analysis of a Stochastic SIR Model with Vaccination and Nonlinear Incidence Rate. *International Journal of Differential Equations* **2019**, *2019*, 9275051.
35. Li, X.; Li, X.; Zhang, Q. Time to extinction and stationary distribution of a stochastic susceptible-infected-recovered-susceptible model with vaccination under. *Mathematical Population Studies* **2020**, *27*, 259–274.
36. Imron, C.; Hariyanto.; Yunus, M.; Surjanto, S.D.; Dewi, N.A.C. Stability and persistence analysis on the epidemic model multi-region multi-patches. *International Conference On Mathematics: Pure, Applied And Computation* **2019**, *1218*, 012035.
37. Britton, T.; Pardoux, E., Eds. *Stochastic Epidemic Models with Inference*; Vol. 2255, Springer, Berlin, 2019; pp. 1–472.
38. Zhang, Y.; Li, Y.; Zhang, Q.; Li, A. Behavior of a stochastic SIR epidemic model with saturated incidence and vaccination rules. *Physica A* **2018**, *501*, 178–187.
39. Xu, C.; Li, X. The threshold of a stochastic delayed SIRS epidemic model with temporary immunity and vaccination. *Chaos Solitons Fract.* **2018**, *111*, 227–234.
40. Liu, Q.; Jiang, D.; Shi, N.; Hayat, T. Dynamics of a stochastic delayed SIR epidemic model with vaccination and double diseases driven by Levy jumps. *Physica A* **2018**, *492*, 2010–2018.
41. Witbooi, P.J. Stability of a Stochastic Model of an SIR Epidemic with Vaccination. *Acta Biotheoretica* **2017**, *65*, 151–165.
42. Miller, J.C. Mathematical models of SIR disease spread with combined non-sexual and sexual transmission routes. *Infectious Disease Modelling* **2017**, *2*, 35–55.
43. Jornet-Sanz, M.; Corberan-Vallet, A.; Santonja, F.J.; Villanueva, R.J. A Bayesian stochastic SIRS model with a vaccination strategy for the analysis of respiratory syncytial virus. *Sort-statistics And Operations Research Transactions* **2017**, *41*, 159–175.
44. Estrada, E. Covid-19 and Sars-Cov-2, Modeling the present, looking at the future. *Phys. Rep.* **2020**, *869*, 1. doi:10.1016/j.physrep.2020.07.005.
45. Schlickeiser, R.; Kröger, M. Determination of a key pandemic parameter of the SIR-epidemic model from past Covid-19 mutant waves and its variation for the validity of the Gaussian evolution. *Physics* **2023**, *5*, 205–214. doi:10.3390/physics5010016.
46. Schlickeiser, R.; Kröger, M. Analytical solution of the Susceptible-Infected-Recovered/Removed model for the not too late temporal evolution of epidemics for general time-dependent recovery and infection rates. *Covid* **2023**, *3*, 1781–1796.
47. Kröger, M.; Schlickeiser, R. Verification of the accuracy of the SIR model in forecasting based on the improved SIR model with a constant ratio of recovery to infection rate by comparing with monitored second wave data. *R. Soc. Open Sci.* **2021**, *8*, 211379. doi:10.1098/rsos.211379.
48. Schlickeiser, R.; Kröger, M. Analytical solution of the SIR-model for the temporal evolution of epidemics. Part B. Semi-time case. *J. Phys. A: Math. Theor.* **2021**, *54*, 175601.
49. Guo, X.; Wang, J.L. A Unified Adsorption Kinetic Model Inspired by Epidemiological Model: Based on Adsorbates "Infect" Adsorbents. *Langmuir* **2024**, *40*, 15569–15579.
50. Guo, X.; Wang, J.L. A novel monolayer adsorption kinetic model based on adsorbates "infect" adsorbents inspired by epidemiological model. *Water Research* **2024**, *253*, 121313.
51. Cui, S.X.; Liu, F.Z.; Jardon-Kojakhmetov, H.; Cao, M. Discrete-time layered-network epidemics model with time-varying transition rates and multiple resources. *Automatica* **2024**, *159*, 111303.

 doi:10.20944/preprints202411.0521.v1

52. Klemm, S.; Ravera, L. On SIR-type epidemiological models and population heterogeneity effects. *Physica A* **2023**, *624*, 128928.
53. Melikechi, O.; Young, A.L.; Tang, T.; Bowman, T.; Dunson, D.; Johndrow, J. Limits of epidemic prediction using SIR models. *Journal of Mathematical Biology* **2022**, *85*, 36.
54. Machado, G.; Baxter, G.J. Effect of initial infection size on a network susceptible-infected-recovered model. *Physical Review E* **2022**, *106*, 014307.
55. Yan, X.R. Research and Practice Analysis of Higher Vocational Colleges Facing the Experience and Dissemination of Regional Characteristic Tea Culture. *Advances In Multimedia* **2022**, *2022*, 2199788.
56. Jayatilaka, R.; Patel, R.; Brar, M.; Tang, Y.; Jisrawi, N.M.; Chishtie, F.; Drozd, J.; Valluri, S.R. A mathematical model of Covid-19 transmission. *Materials Today-proceedings* **2022**, *54*, 101–112.
57. Palomo-Briones, G.A.; Siller, M.; Grignard, A. An agent-based model of the dual causality between individual and collective behaviors in an epidemic. *Computers In Biology And Medicine* **2022**, *141*, 104995.
58. Roman, H.E.; Croccolo, F. Spreading of Infections on Network Models: Percolation Clusters and Random Trees. *Mathematics* **2021**, *9*, 3054.
59. Kavitha, C.; Gowrisankar, A.; Banerjee, S. The second and third waves in India: when will the pandemic be culminated? *European Physical Journal Plus* **2021**, *136*, 596.
60. Di Crescenzo, A.; Gomez-Corral, A.; Taipe, D. A computational approach to extreme values and related hitting probabilities in level-dependent quasi-birth-death processes. *Mathematics And Computers In Simulation* **2025**, *228*, 211–224.
61. Yu, C.; He, J.M.; Ma, Q.T.; Liu, X.Y. Dynamic Evolution Model of Internet Financial Public Opinion. *Information* **2024**, *15*, 433.
62. Athapaththu, D.V.; Ambagaspitiya, T.D.; Chamberlain, A.; Demase, D.; Harasin, E.; Hicks, R.; Mcintosh, D.; Minute, G.; Petzold, S.; Tefft, L.; Chen, J.X. Physical Chemistry Lab for Data Analysis of Covid-19 Spreading Kinetics in Different Countries. *Journal of Chemical Education* **2024**, *101*, 2892–2898.
63. Song, Z.L.; Zhang, Z.; Lyu, F.; Bishop, M.; Liu, J.K.; Chi, Z.H. From Individual Motivation to Geospatial Epidemiology: A Novel Approach Using Fuzzy Cognitive Maps and Agent-Based Modeling for Large-Scale. *Sustainability* **2024**, *16*, 5036.
64. Li, G.J.; Chang, B.F.; Zhao, J.; Wang, J.Y.; He, F.; Wang, Y.H.; Xu, T.; Zhou, Z.G. VIVIAN: virtual simulation and visual analysis of epidemic spread data. *Journal of Visualization* **2024**, *27*, 677–694.
65. Agosto, A.; Cerchiello, P. A data-driven test approach to identify Covid-19 surge phases: an alert-warning tool. *Statistics* **2024**, *58*, 422–436.
66. Yoon, I.; Ahn, C.; Ahn, S.; Lee, B.; Lee, J.; Park, M. Enhancing indoor building occupant safety in the built environment: Assessing the validity of social force modeling for simulating physical. *Developments In The Built Environment* **2024**, *17*, 100336.
67. Yadav, S.K.; Khan, S.A.; Tiwari, M.; Kumar, A.; Kumar, V.; Akhter, Y. Taking cues from machine learning, compartmental and time series models for Sars-Cov-2 omicron infection in Indian provinces. *Spatial And Spatio-temporal Epidemiology* **2024**, *48*, 100634.
68. Finney, L.; Amundsen, D.E. Asymptotic analysis of periodic solutions of the seasonal SIR model. *Physica D-nonlinear Phenomena* **2024**, *458*, 133996.
69. Rocha, J.L.; Carvalho, S.; Coimbra, B. Probabilistic Procedures for SIR and SIS Epidemic Dynamics on Erdös-Rényi Contact Networks. *Appliedmath* **2023**, *3*, 828–850.
70. Ilic, B.; Salom, I.; Djordjevic, M.; Djordjevic, M. An analytical framework for understanding infection progression under social mitigation measures. *Nonlinear Dynamics* **2023**, *111*, 22033–22053.
71. Atienza-Diez, I.; Seoane, L.F. Long- and short-term effects of cross-immunity in epidemic dynamics. *Chaos Solitons Fract.* **2023**, *174*, 113800.
72. Prodanov, D. Computational aspects of the approximate analytic solutions of the SIR model: applications to modelling of Covid-19 outbreaks. *Nonlinear Dynamics* **2023**, *111*, 15613–15631.
73. Darvishi, H.; Darvishi, M.T. An Analytical Study on Two High-Order Hybrid Methods to Solve Systems of Nonlinear Equations. *Journal of Mathematics* **2023**, *2023*, 9917774.
74. Karaji, P.T.; Nyamoradi, N.; Ahmad, B. Stability and bifurcations of an SIR model with a nonlinear incidence rate. *Mathematical Methods In The Applied Sciences* **2023**, *46*, 10850–10866.
75. Chakir, Y. Global approximate solution of SIR epidemic model with constant vaccination strategy. *Chaos Solitons Fract.* **2023**, *169*, 113323.

 doi:10.20944/preprints202411.0521.v1

76. Salimipour, A.; Mehraban, T.; Ghafour, H.S.; Arshad, N.I.; Ebadi, M.J. SIR model for the spread of Covid-19: A case study. *Operations Research Perspectives* **2023**, *10*, 100265.
77. Luangwilai, T.; Thammawichai, M. Optimal river flow management to reduce flood risks: A case study in northeastern Thailand. *River Research And Applications* **2023**, *39*, 255–265.
78. Prodanov, D. Asymptotic analysis of the SIR model and the Gompertz distribution. *Journal of Computational And Applied Mathematics* **2023**, *422*, 114901.
79. Qin, Y.P.; Wang, Z.; Zou, L. Analytical properties and solutions of a modified Lindemann mechanism with three reaction rate constants. *Journal of Mathematical Chemistry* **2023**, *61*, 389–401.
80. Ishfaq, U.; Khan, H.U.; Iqbal, S. Identifying the influential nodes in complex social networks using centrality-based approach. *Journal of King Saud University-computer And Information Sciences* **2022**, *34*, 9376–9392.
81. Gairat, A.; Shcherbakov, V. Discrete SIR model on a homogeneous tree and its continuous limit. *Journal of Physics A* **2022**, *55*, 434004.
82. Al-Obaidi, R.H.; Darvishi, M.T. Constructing a Class of Frozen Jacobian Multi-Step Iterative Solvers for Systems of Nonlinear Equations. *Mathematics* **2022**, *10*, 2952.
83. Öz, Y. Analytical investigation of compartmental models and measure for reactions of governments. *European Physical Journal E* **2022**, *45*, 68.
84. de Souza, D.B.; Araújo, H.A.; Duarte, G.C.; Gaffney, E.A.; Santos, F.A.N.; Raposo, E.P. Fock-space approach to stochastic susceptible-infected-recovered models. *Physical Review E* **2022**, *106*, 014136.
85. Kozyreff, G. Asymptotic solutions of the SIR and SEIR models well above the epidemic threshold. *Ima Journal of Applied Mathematics* **2022**, *87*, 521–536.
86. Tchoumi, S.Y.; Rwezaura, H.; Tchuenche, J.M. Dynamic of a two-strain Covid-19 model with vaccination. *Results In Physics* **2022**, *39*, 105777.
87. Schwarzendahl, F.J.; Grauer, J.; Liebchen, B.; Löwen, H. Mutation induced infection waves in diseases like Covid-19. *Scientific Reports* **2022**, *12*, 9641.
88. Gulec, F.; Atakan, B.; Dressler, F. Mobile human ad hoc networks: A communication engineering viewpoint on interhuman airborne pathogen transmission. *Nano Communication Networks* **2022**, *32-33*, 100410.
89. Turkyilmazoglu, M. A restricted epidemic SIR model with elementary solutions. *Physica A* **2022**, *600*, 127570.
90. Turkyilmazoglu, M. An extended epidemic model with vaccination: Weak-immune SIRV I. *Physica A* **2022**, *598*, 127429.
91. d'Andrea, V.; Gallotti, R.; Castaldo, N.; De Domenico, M. Individual risk perception and empirical social structures shape the dynamics of infectious disease outbreaks. *Plos Computational Biology* **2022**, *18*, e1009760.
92. Jiang, J.Y.; Zhou, Y.C.; Chen, X.S.; Jhou, Y.R.; Zhao, L.Q.; Liu, S.; Yang, P.C.; Ahmar, J.; Wang, W. COVID-19 Surveiller: toward a robust and effective pandemic surveillance system basedon social media mining. *Philosophical Transactions of The Royal Society A-mathematical Physical* **2022**, *380*, 20210125.
93. Uçar, D.; Çelik, E. Analysis of Covid 19 disease with SIR model and Taylor matrix method. *Aims Mathematics* **2022**, *7*, 11188–11200.
94. Berenbrink, P.; Cooper, C.; Gava, C.; Marzagao, D.K.; Mallmann-Trenn, F.; Radzik, T. On Early Extinction and the Effect of Travelling in the SIR model. *Uncertainty In Artificial Intelligence, Vol 180* **2022**, *180*, 159–169.
95. Hussain, S.; Madi, E.N.; Khan, H.; Etemad, S.; Rezapour, S.; Sitthiwirattham, T.; Patanarapeelert, N. Investigation of the Stochastic Modeling of Covid-19 with Environmental Noise from the Analytical and Numerical Point of View. *Mathematics* **2021**, *9*, 3122.
96. Rusu, A.C.; Emonet, R.; Farrahi, K. Modelling digital and manual contact tracing for Covid-19. Are low uptakes and missed contacts deal-breakers? *Plos One* **2021**, *16*, e0259969.
97. Lee, K.; Parish, E.J. Parameterized neural ordinary differential equations: applications to computational physics problems. *Proceedings of The Royal Society A-mathematical Physical And Engineering* **2021**, *477*, 20210162.
98. Bärwolff, G. A Local and Time Resolution of the Covid-19 Propagation-A Two-Dimensional Approach for Germany Including Diffusion Phenomena to. *Physics* **2021**, *3*, 536–548.
99. Kartono, A.; Karimah, S.V.; Wahyudi, S.T.; Setiawan, A.A.; Sofian, I. Forecasting the Long-Term Trends of Coronavirus Disease 2019 (COVID-19) Epidemic Using the Susceptible-Infectious-Recovered (SIR) Model. *Infectious Disease Reports* **2021**, *13*, 668–684.

 doi:10.20944/preprints202411.0521.v1

100. Hynd, R.; Ikpe, D.; Pendleton, T. Two critical times for the SIR model. *Journal of Mathematical Analysis And Applications* **2022**, *505*, 125507.
101. Zhou, Y.C.; Jiang, J.Y.; Chen, X.S.; Wang, W. #StayHome or #Marathon? Social Media Enhanced Pandemic Surveillance on Spatial-temporal Dynamic Graphs. *Proceedings of The 30th Acm International Conference On Information* **2021**, pp. 2738–2748.
102. Schüttler, J.; Schlickeiser, R.; Schlickeiser, F.; Kröger, M. Covid-19 predictions using a Gauss model, based on data from April 2. *Physics* **2020**, *2*, 197–202.
103. Kröger, M.; Turkyilmazoglu, M.; Schlickeiser, R. Explicit formulae for the peak time of an epidemic from the SIR model. Which approximant to use? *Physica D* **2021**, *425*, 132981.
104. Lambert, J.H. Observations variae in Mathesin Puram, Acta Helvitica. *Phys. Math. Anatom. Botan Med.* **1758**, *3*, 128–168.
105. Kröger, M.; Schlickeiser, R. Analytical solution of the SIR-model for the temporal evolution of epidemics. Part A: Time-independent reproduction factor. *J. Phys. A: Math. Theor.* **2020**, *53*, 505601.
106. Haas, F.; Kröger, M.; Schlickeiser, R. Multi-Hamiltonian structure of the epidemics model accounting for vaccinations and a suitable test for the accuracy of its numerical solvers. *J. Phys. A* **2022**, *55*, 225206.
107. Weisstein, E. *The CRC Encyclopedia of Mathematics, Third Edition*; Chapman and Hall/CRC Press, Boca Raton, Florida, United States, 2009.
108. Beyer, W.H. *CRC Standard Mathematical Tables, 28th ed.*; CRC Press, Boca Raton, Florida, United States, 1987; p. 455.
109. Shampine, L.F.; Reichelt, M.W. The MATLABODE suite. *SIAM J. Sci. Comput.* **1997**, *18*, 1–22.
110. Bender, C.; Ghosh, A.; Vakili, H.; Ghosh, P.; Ghosh, A.W. An effective drift-diffusion model for pandemic propagation and uncertainty prediction. *Biophysical Reports* **2024**, *4*, 100182.
111. Jang, G.H.; Kim, S.J.; Lee, M.J.; Son, S.W. Effectiveness of vaccination and quarantine policies to curb the spread of Covid-19. *Physica A* **2024**, *637*, 129580.
112. Gao, W.H.; Wang, Y.; Cao, J.D.; Liu, Y. Final epidemic size and critical times for susceptible-infectious-recovered models with a generalized contact rate. *Chaos* **2024**, *34*, 013152.
113. Dobie, A.P.; Bayrakal, A.; Or, M.E.; Bilge, A.H. Dynamics of Feline Coronavirus and FIP: A Compartmental Modeling Approach. *Veterinary Medicine International* **2023**, *2023*, 2721907.
114. Shirazian, M. A new acceleration of variational iteration method for initial value problems. *Mathematics And Computers In Simulation* **2023**, *214*, 246–259.
115. Turkyilmazoglu, M. A highly accurate peak time formula of epidemic outbreak from the SIR model. *Chinese Journal of Physics* **2023**, *84*, 39–50.
116. Alshammari, F.S. Analysis of SIRV I model with time dependent coefficients and the effect of vaccination on the transmission rate and Covid- 19 epidemic waves. *Infectious Disease Modelling* **2023**, *8*, 172–182.
117. Dimou, A.; Maragakis, M.; Argyrakis, P. A network SIRX model for the spreading of Covid-19. *Physica A* **2022**, *590*, 126746.
118. Wang, Q.B.; Wu, H. There exists the 'smartest' movement rate to control the epidemic rather than 'city lockdown'? *Applied Mathematical Modelling* **2022**, *106*, 696–714.
119. Gölgeli, M. The contagion dynamics of vaccine skepticism. *Hacettepe Journal of Mathematics And Statistics* **2022**, *51*, 1697–1709.
120. Wang, S.F.; Ma, Z.H.; Li, X.H.; Qi, T. A generalized delay-induced SIRS epidemic model with relapse. *Aims Mathematics* **2022**, *7*, 6600–6618.
121. Harko, T.; Lobo, F.S.N.; Mak, M.K. Exact analytical solutions of the susceptible-infected-recovered (SIR) epidemic model and of the SIR model with equal death and birth rates. *Appl. Math. Comput.* **2014**, *236*, 184–194.